THE JOURNAL OF PHYSICAL CHEMISTRY C

Article

pubs.acs.org/JPCC

Excited State and Injection Dynamics of Triphenylamine Sensitizers Containing a Benzothiazole Electron-Accepting Group on TiO_2 and Al_2O_3 Thin Films

Mihalis Fakis,*[,†] Peter Hrobárik,*[,‡] Oleksandr Yushchenko,[∥] Ivica Sigmundová,[§] Marius Koch,[∥] Arnulf Rosspeintner,[∥] Elias Stathatos,[⊥] and Eric Vauthey*[,∥]

[†]Department of Physics, University of Patras, GR-26500 Patras, Greece

[‡]Institute of Chemistry, Technical University of Berlin, Strasse des 17. Juni 135, D-10623 Berlin, Germany

[§]Department of Organic Chemistry, Faculty of Natural Sciences, Comenius University, Mlynská dolina, SK-84215 Bratislava, Slovakia

[∥]Physical Chemistry Department, University of Geneva, 30 Quai Ernest Ansermet, CH-1211 Geneva, Switzerland

[⊥]Electrical Engineering Department, Technological Educational Institute of Patras, GR-26334 Patras, Greece

Supporting Information

ABSTRACT: The excited state and electron injection dynamics of three new organic sensitizers, comprising a triphenylamine moiety connected by an ethenylene (C−C double-bond) or ethynylene (C−C triple-bond) π-spacer to an electron-withdrawing benzothiazole bearing a cyanoacrylic acid anchoring group, have been studied using a combination of steady-state and femtosecond-resolved spectroscopies. The measurements were carried out for the three dyes in predominantly neutral and completely deprotonated forms in liquid solutions and bound on nanocrystalline TiO_2 and Al_2O_3 thin films. In addition, quantum-chemical calculations were performed to predict absorption spectra of the sensitizers and their corresponding cation radicals. Time-resolved fluorescence (TRF) measurements on TiO_2 indicate that electron injection takes place on a <0.2 ps time scale. Transient electronic absorption (TA) measurements provide evidence for the formation of radical cations not only in dye-sensitized TiO_2 films but also in Al_2O_3 ones. The cation lifetime in Al_2O_3 is significantly shorter compared to TiO_2, indicating a faster recombination of injected electrons with the dye cations. In addition, the ground-state bleach band in dye-sensitized TiO_2 films experiences a gradual red-shift, which is indicative of a transient Stark effect. Finally, femtosecond transient absorption measurements in the IR region point to an ultrafast generation of injected electrons for all dyes. A faster recombination of the injected electrons with the dye cations is observed for the sensitizer decorated with auxiliary electron-donating methoxy groups on the triphenylamine moiety.

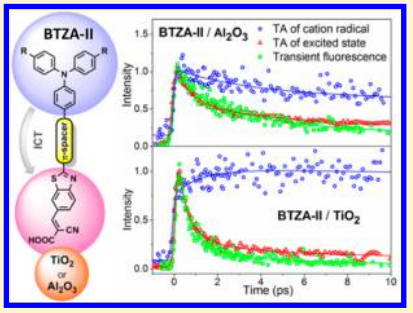

INTRODUCTION

Dye-sensitized solar cells (DSSCs), composed of a wide band gap semiconductor (typically TiO_2 or ZnO) and a dye absorbing in the visible spectral region, have recently reached photoconversion efficiency exceeding 12%, by using cobalt-based redox couples. However, a considerable progress toward the improvement of device efficiency and stability can still be achieved through better understanding and optimization of the fundamental charge-transfer processes.[1,2] In a working DSSC, a variety of kinetically competing charge-transfer mechanisms take place.[3] The rate of each process depends on the energy levels at the interfaces, the materials used, their morphology, and preparation conditions as well as the chemical interactions between them. The most fundamental process in DSSCs, after the absorption of light by the dye molecules, is the electron injection from the dye's excited state to the conduction band of the wide band gap semiconductor. It depends on: (i) the free-energy difference between the dye's excited state and the semiconductor's conduction band (driving force), (ii) the electronic coupling between the dye and the semiconductor, and (iii) the density of states of the electron-accepting sites in the semiconductor.[4] Electron injection in sensitized semiconductor films without the electrolyte has been found to exhibit multiphasic dynamics on the 100 fs time scale and is thus much faster than electron−hole recombination on the dye molecule.[5−11] Recent studies have shown that in complete DSSCs, i.e., in the presence of electrolyte, electron injection is retarded, taking place on the 10−100 ps time scale, because of a positive shift of the energy of the semiconductor's conduction band due to the interaction with the electrolyte.[12−16]

Femtosecond spectroscopy is a most valuable tool to determine the rate of the various carrier transfer dynamics taking place in liquid as well as in solid-state DSSCs. More specifically, femtosecond transient absorption (TA)[7,11,12,14,17−22] and time-resolved fluorescence (TRF)[8,10,13,23−27] spectroscopies are the most widely used

Received: October 2, 2014
Revised: November 14, 2014
Published: November 15, 2014

techniques in these studies. Although TA measurements allow us to identify the generation of dye cations formed after injection of electrons from the dye's excited state to the conduction band of the semiconductor, the corresponding TA spectra can contain overlapping contributions from other species such as excited molecules and/or injected electrons. TA spectroscopy can also provide evidence for the existence of Stark effects which arise after electron injection, affecting the properties of dye molecules and cations.[6,11,17,28] On the other hand, femtosecond TRF spectroscopy monitors only the relaxation of the excited state(s) of the dye molecule. Additionally, femtosecond transient IR spectroscopy is the most straightforward technique to probe the generation of the injected electrons in the conduction band of the oxide semiconductor.[14,21] All the above techniques can be considered complementary and their synergetic application to the study of electron injection and recombination dynamics is the most suitable and reliable procedure.

As far as the sensitizers are concerned, numerous studies have shown that all-organic sensitizers with a D-π-A, D-π-D-π-A, or D-π-A-π-A structure, where D and A are electron-donating and -withdrawing groups, respectively, offer several advantages over organometallic complexes, such as higher molar extinction coefficients, easier synthesis, and reduced production cost.[29−40] Moreover, their use does not rely on the availability of precious metals like ruthenium, osmium, or iridium. The choice of electron-donating and -accepting groups and of the π-bridge allows a specific tailoring of optical and electronic properties to match the criteria needed for improving the DSSC efficiency and stability. In this respect, a benzothiazole unit could be an attractive building block for sensitizers because of its electron-withdrawing character and increased chemical and photophysical stability. Interestingly, this heterocyclic scaffold has been so far only scarcely used in organic sensitizers,[41] although it has been successfully employed in various functional materials, such as organic compounds displaying enhanced nonlinear optical properties.[42−48]

In this paper, we present a detailed investigation of three new triphenylamine-benzothiazole sensitizers (Figure 1) by combining steady-state spectroscopy, femtosecond time-resolved fluorescence spectroscopy and femtosecond transient absorption spectroscopy in the visible and IR regions. All these techniques provide an insight into the dynamics of the excited state, the electron injection, the photoinduced radical cation generation, and the formation of free electrons in the conduction band. Quantum chemical calculations have also been performed in order to predict the cation absorption spectra, which were needed for a better interpretation of the TA spectra. Investigations have been conducted with the three sensitizers in $CHCl_3$ solutions in the absence and presence of a base, respectively, and on nanocrystalline TiO_2 and Al_2O_3 films. The studies are focused on (a) a comparison of the photodynamics in the different environments and (b) a comparison of the photodynamics of the three dyes in order to predict which structure seems more suitable for solar cell applications.

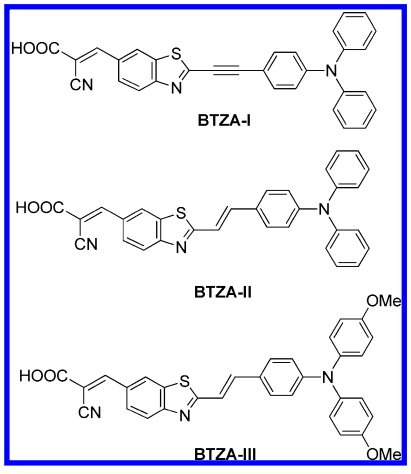

Figure 1. Structure of the triphenylamine-benzothiazole sensitizers **BTZA-I−III**.

EXPERIMENTAL SECTION

Materials. *Dyes.* The structures of the sensitizers investigated here, along with their abbreviations, are shown in Figure 1. All three compounds consist of a triphenylamine moiety (with or without auxiliary electron-donating methoxy groups) coupled by a π-spacer to the benzothiazole ring bearing a cyanoacrylic acid anchoring group. The synthetic procedures and spectroscopic characterization of the sensitizers are described in the Supporting Information.

The solvent used for the spectroscopic measurements, chloroform ($CHCl_3$), was of spectrophotometric grade (Sigma-Aldrich, ≥99.8%). The purity of the base, 1,8-diazabicyclo[5.4.0]undec-7-ene (DBU, Fluka Analytical), was higher than 99%.

Preparation of the Al_2O_3 and TiO_2 Films. The details for the preparation of the nanocrystalline Al_2O_3 and TiO_2 films have been published elsewhere.[10] Briefly, for Al_2O_3 thin films, two solutions were prepared in separate containers. The first solution consisted of the nonionic surfactant Triton X-100 (0.21 g) dissolved in ethanol (9 mL) and the second of aluminum *sec*-butoxide $Al(O^sBu)_3$ (0.09 g) dissolved in water (3 mL) with pH adjusted to 2 using HCl acid. The solutions were mixed, and the mixture was stirred for an hour and then aged for 1 day. For TiO_2 films, Triton X-100 (1.8 g) was mixed with ethanol (10 mL), followed by addition of glacial acetic acid (0.8 mL) and titanium isopropoxide $Ti(O^iPr)_4$ (0.9 mL) under vigorous stirring. For preparing the films, conductive glass substrates (fluorine-doped SnO_2, FTO) were dipped in the above solutions and withdrawn with a rate of 2 cm/s. Both TiO_2 and Al_2O_3 films were heated to 500 °C for 30 min with a 20 °C/min heating ramp rate. A final film thickness of around 1.5 μm was achieved (based on evidence of cross-sectional SEM images). These films, after being sensitized with the dyes, have shown good optical transparency in the visible region and at 4000 nm and have been used in all spectroscopic studies herein.

Samples. The three sensitizers have been studied in $CHCl_3$ solutions in the absence and presence of DBU base, respectively, and on nanocrystalline TiO_2 and Al_2O_3 films. For TA measurements the concentration of the solutions was adjusted so that the optical density in a 1 mm cuvette was ∼0.2 at the excitation wavelength. The solutions in the presence of DBU have been prepared by adding an equimolar amount of DBU to the $CHCl_3$ solutions. The sensitized films were prepared by immersing the TiO_2 and Al_2O_3 films in a 5×10^{-4} M solution of the dyes in $CHCl_3$ (immersing time 15 min). The TiO_2 and Al_2O_3 dye-sensitized films were measured in air several weeks after the immersion in dye solutions and over a

dx.doi.org/10.1021/jp509971q | J. Phys. Chem. C 2014, 118, 28509−28519

period of one month. No significant difference was observed in the dynamics. TiO_2 has been used to study electron injection from the dyes to its conduction band (located at ∼−0.5 V vs NHE, i.e., lower than the excited state potential of the dyes), while the potential of the conduction band of Al_2O_3 is higher than the excited state potential of the dyes (−4.5 V vs NHE).

Computational Details. The ground-state structure optimizations were carried out using density functional theory (DFT) at the B3LYP/TZVP level as implemented in the Gaussian 09 package.[49] For the radical cations, the unrestricted Kohn−Sham formalism was used. Harmonic vibrational frequencies have been computed for both the neutral and deprotonated forms of the sensitizers to prove that the optimized structures are minima on the potential energy surface. Vertical excitation energies were calculated by time-dependent DFT, using the modified CAM-B3LYP functional[50] with the following parameters: $\alpha = 0.19$, $\beta = 0.33$, $\gamma = 0.33$, and the TZVP basis set for all atoms. Bulk solvent effects were simulated using the integral equation formalism of the polarizable continuum model (IEF-PCM).[51] For each of the molecules, a number of conformational isomers were examined, and the computed excitation energies were Boltzmann-averaged (at 298 K). To facilitate the visualization and to allow an easier comparison with experiment, the calculated absorption spectra were convolved with a Gaussian function having a full width at half-maximum (fwhm) of 0.2 eV.

Steady-State Measurements. The steady-state absorption and fluorescence spectra of the compounds in films were obtained using a Hitachi U-2900 UV−vis and a Hitachi F-2500 fluorescence spectrophotometer, respectively. The accuracy of the steady-state fluorescence measurements was checked using the Europium Eu^{3+} emission ($^5D_0 \rightarrow {}^7F_2$ transition) at 613 nm as a reference. The fluorescence spectra of solid samples were collected using a special holder with a 10° inclination angle, thus avoiding increased reflections of the excitation beam toward the detection pathway.

Femtosecond TRF Measurements. The fluorescence dynamics have been studied using femtosecond time-resolved upconversion spectroscopy, with a setup described in detail previously.[10,26] The second harmonic of a Ti:sapphire femtosecond laser was used as the excitation beam (400 nm wavelength, 80 MHz repetition rate, <5 mW average power). The fluorescence of the samples was collected and mixed together with the delayed fundamental beam (800 nm) on a type I BBO crystal to produce a UV signal beam, which was then passed through appropriate filters and a monochromator and was detected by a photomultiplier connected to a computer. The polarization between the excitation and the detection was set to magic angle. The instrument response function (IRF) was about 140 fs. The dynamics were reconstructed after averaging of three to five decay curves.

Femtosecond TA Measurements. *In the Visible Region.* The electronic TA setup has been described in detail previously.[52,53] The 800 nm and 150 fs output pulses (FWHM) of an amplified Ti:sapphire system were split into two parts. One part was used for white light generation, from 360 to 750 nm, after focusing into a 3 mm thick CaF_2 window. The other fraction was either frequency doubled to generate the 400 nm excitation beam or used to pump a noncollinear optical parametric amplifier (NOPA) to generate the excitation beam at 505 nm. The fluence of the excitation beam at the sample was approximately 0.1 mJ/cm^2, and its polarization was at magic angle with respect to the probe beam. TA measurements were performed from −5 up to 1700 ps. The solid samples were placed in a holder, which was constantly moved randomly, on a plane perpendicular to the excitation beam. The liquid samples were measured in a 1 mm quartz cell and bubbled continuously by N_2 during all measurements. The TA spectra were corrected for the chirp of the white-light probe pulses, and a global fitting method has been used for their analysis. The fitting routine did not account for a wavelength-dependent IRF. Therefore, the first ca. 300 fs were excluded from the analysis, to avoid artifacts arising from the IRF.

In the Infrared Region. The experimental setup for fs IR TA experiments was based on a Ti:sapphire amplified system (Spectra Physics Solstice) producing 100 fs pulses at 800 nm at 1 kHz.[54] Excitation was performed with 0.02 μJ pulses at 400 nm produced by frequency doubling a fraction of the amplifier output and focused to a 350 μm diameter spot on the sample (∼0.02 mJ/cm^2). Mid-IR probe pulses at around 4 μm were generated by difference frequency mixing the output of an optical parametric amplifier (Light Conversion, TOPAS-C with NDFG module) pumped at 800 nm. The polarization of the IR beam was controlled using a wire-grid polarizer. Two horizontally polarized beams were produced by means of a CaF_2 wedge and focused onto the sample to a 140 μm diameter spot. One of the beams was overlapped with the pump beam and polarized at magic angle with respect to the pump beam, whereas the second was used as a reference beam. Both IR beams were focused onto the entrance slit of an imaging spectrograph (Horiba, Triax 190, 150 lines/mm) equipped with a liquid nitrogen cooled 2 × 64 element MCT array (Infrared Systems Development).

The sample area and the detection system were located in a box that was purged with dry air for at least 45 min before each experiment. The average of 2000 signal shots was taken to collect one data point. For each system, six to eight measurements were averaged to reconstruct the spectra. The solid sample was moved between each measurement, and no sample degradation was observed during one measurement, as controlled by identical amplitudes before and after every measurement at a time delay of 1 ps. The IR signal at each time delay is an average over 14 MCT pixels (60 cm^{-1}).

RESULTS AND DISCUSSION

Steady-State Absorption and Fluorescence Spectra. The steady-state absorption and fluorescence spectra of the triphenylamine-benzothiazole sensitizers in different environments are shown in Figures 2a−d. For comparative purposes, the spectra of **BTZA-II** measured in $CHCl_3$ solution and on the Al_2O_3 and TiO_2 surface are provided in Figure S1 (Supporting Information). The photophysical parameters of all three compounds are summarized in Table 1. In general, the three sensitizers display two intense absorption bands. On the basis of TD-DFT calculations, the lower-energy band appearing at 410−490 nm is primarily associated with the HOMO−LUMO transition and corresponds to an intramolecular-charge transfer (ICT) from the arylamine moiety to the electron-withdrawing benzothiazole and adjacent cyanoacrylic acid group (see Figure 3 for the frontier molecular orbitals of **BTZA-II**). The higher-energy band located at around 350−370 nm is assigned to delocalized $\pi-\pi^*$ HOMO−1 → LUMO and HOMO → LUMO+1 transitions (cf. Figure 3).

A significant red shift of both absorption (λ_{abs}) and emission (λ_f) peaks, by 53 and 38 nm (0.34 and 0.15 eV), respectively, is observed when going from **BTZA-I** to **BTZA-II**, indicating that

dx.doi.org/10.1021/jp509971q | J. Phys. Chem. C 2014, 118, 28509−28519

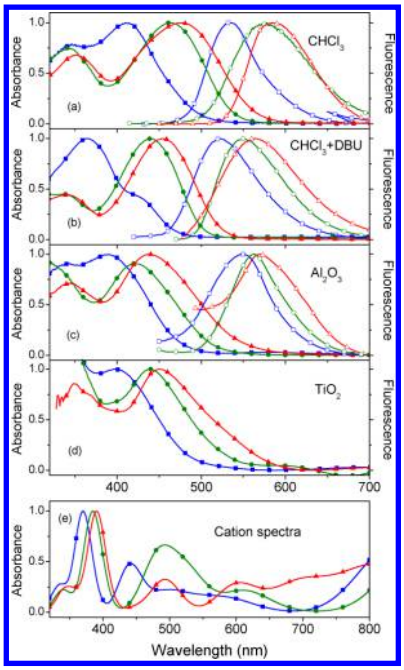

Figure 2. (a), (b), (c), (d) Normalized absorption (full points) and fluorescence (empty points) spectra of **BTZA-I** (blue squares), **BTZA-II** (green circles), and **BTZA-III** (red triangles) in different environments. (e) Calculated absorption spectra of the dye radical cations. The intensity of the steady-state fluorescence spectra on TiO_2 was too small to be measured.

π-conjugation via an ethenylene (C═C double bond) spacer is energetically more favorable than that through an alkyne-type (C≡C triple bond) bridge. Both λ_{abs} and λ_f are further red-shifted by 12 and 11 nm (0.07 and 0.04 eV), respectively, upon introducing an auxiliary donor functionality (methoxy group) onto the triphenylamine moiety (cf. **BTZA-II** vs **BTZA-III**).

The absorption spectra of the dyes on solid substrates display a remarkable blue shift of ICT absorption maxima ranging from 21 to 42 nm (0.16 to 0.26 eV) as compared to the spectra measured in $CHCl_3$. This hypsochromic shift can be primarily ascribed to the deprotonation of the carboxylic group and attachment of dye molecules via carboxylate oxygen atom(s) to the TiO_2 surface. A similar but less pronounced blue shift is also observed in the fluorescence spectra of Al_2O_3 samples except from the case of **BTZA-I**. It is worth noting that the fluorescence of all compounds on the TiO_2 surface was dramatically quenched due to efficient electron injection, which prevented us from measuring the emission spectra of the TiO_2 samples.

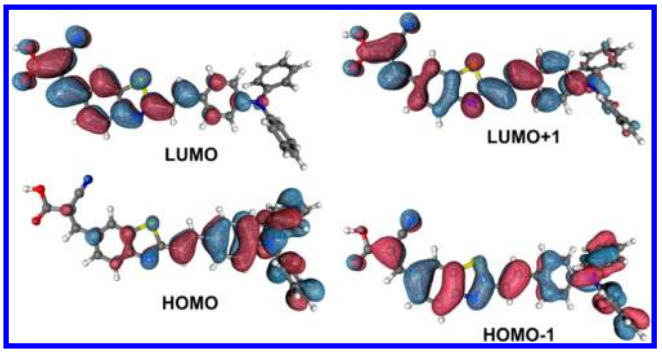

Figure 3. Frontier molecular orbitals of **BTZA-II**.

To examine the effect of deprotonation of the carboxylic COOH group on the photophysical properties of the "free" (covalently nonbonded) dyes, solutions in the presence of strong organic base (DBU) were studied as well.[55] Adding DBU shifts the equilibrium almost exclusively toward the anionic (COO^-) form, which displays a blue-shift of the ICT absorption band by ca. 23−46 nm (0.13−0.38 eV) as compared to the predominantly "nondeprotonated" dye molecules in $CHCl_3$ solution (cf. Table 1). This remarkable change of ICT characteristics upon deprotonation also coincides with the excitation energies computed for neutral and anionic forms of the dyes (Table 1).

The calculated absorption spectra of the sensitizer cations in the wavelength range of 320−800 nm are presented in Figure 2e. They display three main bands located at 380−400 nm, 440−500 nm, and at 580−650 nm, while $[\mathbf{BTZA\text{-}III}]^+$ also exhibits a pronounced absorption at λ around 700 nm. In addition, all cation radicals derived from **BTZA-I−III** are predicted to show also a distinct absorption band at longer wavelengths with maxima at 820−900 nm, which are, however, outside the experimental spectral window.

Time-Resolved Fluorescence Dynamics. TRF measurements have been performed for the dyes on TiO_2 and Al_2O_3 substrates in order to investigate the electron injection dynamics. Figures 4a and 4b show the fluorescence dynamics measured for **BTZA-II** on TiO_2 and Al_2O_3 films, respectively, at different emission wavelengths. The decays have been fitted by a three-exponential decay function convolved with the IRF and the parameters are given in Table 2. The average lifetimes have been determined as $\langle\tau\rangle = [(\sum_i A_i\tau_i)/(\sum_i A_i)]$. The dynamics for compounds **BTZA-I** and **BTZA-III** on TiO_2 and Al_2O_3 are shown in Figure S2, and the results are summarized in Table S1 (Supporting Information).

The fluorescence dynamics of **BTZA-II** on TiO_2 show an ultrafast decay component (0.19−0.60 ps depending on the

Table 1. ICT Absorption and Fluorescence Characteristics of the Benzothiazole-derived Sensitizers BTZA-I−III

dye	λ_{abs} (nm)				λ_f (nm)			λ_{abs}^{calcd} (nm)[d]	
	$CHCl_3$		Al_2O_3	TiO_2	$CHCl_3$		Al_2O_3	neutral	anion
	c = 25 μM[a]	+ DBU[b]			c = 25 μM[a]	+ DBU[b]			
BTZA-I	411 (84500)[c]	365	390	398	535	522	549	439	395
BTZA-II	464 (30960)[c]	440	422	440	573	549	563	461	412
BTZA-III	476 (57720)[c]	453	438	450	584	564	570	480	427

[a]Due to the acid−base equilibrium between the dissociated and non-dissociated form of the sensitizer, the absorption and emission peak positions depend also on the dye concentration. The data presented here are given for 25 μM solutions in $CHCl_3$. [b]Absorption and emission maxima measured after adding an equimolar amount of DBU to the chloroform solution of the sensitizer. [c]Molar extinction coefficients given in $M^{-1}cm^{-1}$. [d]Vertical excitation energies calculated at the mCAM-B3LYP/TZVP level using a PCM solvation model (cf. Computational Details).

dx.doi.org/10.1021/jp509971q | J. Phys. Chem. C 2014, 118, 28509−28519

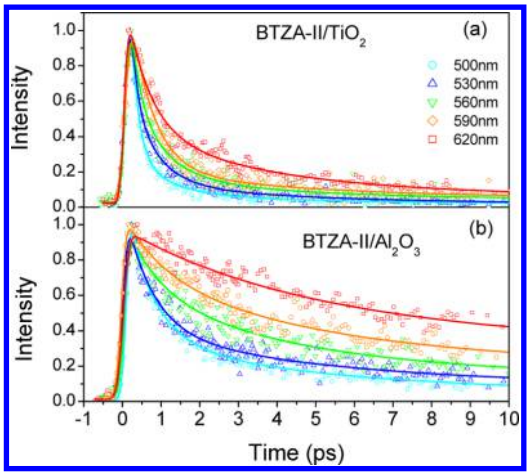

Figure 4. Fluorescence decay dynamics measured for **BTZA-II** on (a) TiO_2 and (b) Al_2O_3 substrates at various detection wavelengths upon 400 nm excitation. The dynamics were reconstructed after averaging three to five decay curves.

detection wavelength, cf. Table 2), indicating an ultrafast electron injection, whereas slower components have also been found. The wavelength dependence is due to the fact that faster electron injection takes place from energetically higher-lying excited state sublevels, while slower electron injection takes place from lower ones. Apart from **BTZA-II**, ultrafast decay components have been also found for **BTZA-I** and **BTZA-III** on TiO_2 (τ_1 = 0.18 and 0.10 ps for **BTZA-I** and **BTZA-III**, respectively; cf. Table S1, Supporting Information). Similar multiexponential decays have been reported in the past for other D-π-A dye/coated TiO_2 films exhibiting ultrafast as well as picosecond electron injection dynamics.[6,8,10,18,56] The multiexponential decays, indicating a multiphasic injection mechanism, are mainly associated with the inhomogeneity of the dye-coated films, i.e., different concentration of the adsorbed dye molecules at different spots of the films, coexistence of isolated dye molecules and aggregates, etc. All these species inject electrons at different rate constants. In addition, electron injection from both unrelaxed and relaxed excited states also leads to multiexponential injection with the relaxed state being responsible for a delayed injection because of its lower energetic position. By examining the TRF results, it is also concluded that the average lifetimes of the sensitizers on Al_2O_3 are longer than on TiO_2. However, even in Al_2O_3 samples, relatively fast decay times are found (τ_1 for **BTZA-II** ranges from 0.18 to 1.0 ps for wavelengths from 500 to 590 nm, Table 2), indicating that electron injection into trap states may occur to some extent (*vide infra*). Besides, slower dynamic features with 40−100 ps time constants have been obtained in Al_2O_3. These are assigned to non-electron-injecting species, responsible for the fluorescence spectra shown in Figure 2c.

Transient Absorption Dynamics in the Visible. The TA spectra of the three sensitizers **BTZA-I−III** were measured on Al_2O_3 and TiO_2 substrates upon excitation at 400 and 505 nm. For comparison, the TA spectra were also measured in $CHCl_3$ solutions with and without DBU base. Figures 5a, 6a, and 7a show the TA spectra measured for **BTZA-II** in $CHCl_3$ + DBU, on Al_2O_3 and TiO_2 at various time delays. The reverse absorption and stimulated emission (SE) spectra are also shown for comparison. The latter were calculated by multiplying the spontaneous emission spectra by λ^4.[57] The parameters of the TA dynamics, obtained after a multiexponential global analysis, are summarized in Table 3, and the Decay Associated Difference Spectra (DADS) are shown in Figures 5b, 6b, and 7b.

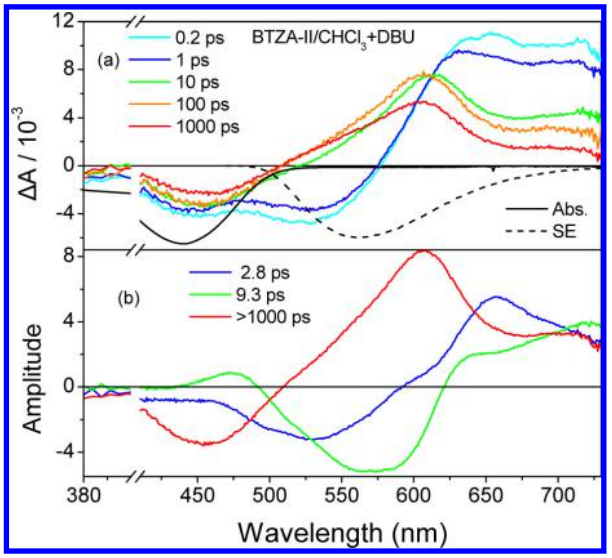

Figure 5. (a) TA spectra measured for **BTZA-II** in $CHCl_3$ in the presence of DBU at different time delays upon 400 nm excitation. The reverse absorption and SE spectra are also shown for comparison. (b) DADS obtained after a three exponential global analysis.

Table 2. Fluorescence Decay Parameters for BTZA-II on TiO_2 and Al_2O_3 Substrates at Various Wavelengths Obtained from Multiexponential Analysis[a]

λ_{em} (nm)	substrate	A_1	τ_1 (ps)	A_2	τ_2 (ps)	A_3	τ_3 (ps)	$\langle\tau\rangle$ (ps)
500	TiO_2	0.82	0.10	0.15	0.88	0.03	4.7	0.36
530		0.59	0.10	0.35	0.90	0.06	4.5	0.70
560		0.53	0.15	0.38	0.70	0.09	4.6	0.80
590		0.84	0.58	0.12	3.3	0.04	13	1.4
620		0.62	0.60	0.31	3.3	0.07	20	2.8
500	Al_2O_3	0.30	0.18	0.49	0.74	0.21	5.2	1.5
530		0.42	0.20	0.60	1.0	0.26	8.7	2.9
560		0.38	1.2	0.48	5.0	0.14	38	8.2
590		0.30	1.2	0.50	4.4	0.20	45	12
620		0.54	4.8	0.19	18	0.27	100	33

[a]All decay parameters have been obtained after fitting to the average of three to five decay curves and contain an error of less than 10%.

dx.doi.org/10.1021/jp509971q | J. Phys. Chem. C 2014, 118, 28509−28519

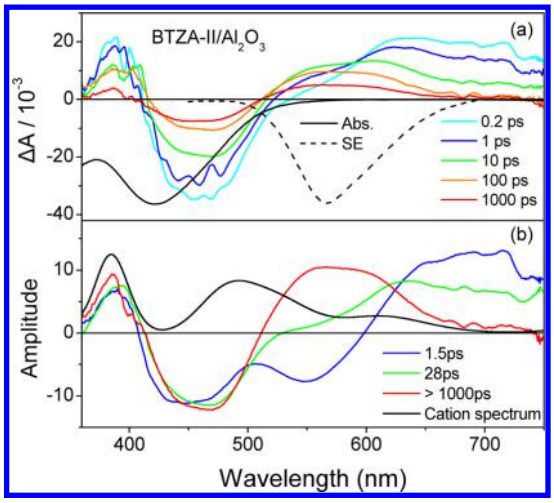

Figure 6. (a) TA spectra measured for **BTZA-II** on Al_2O_3 substrate at different time delays upon 400 nm excitation. The reverse absorption and SE spectra are also shown for comparison. (b) DADS obtained after a three exponential global analysis. The calculated radical cation spectrum is shown in (b).

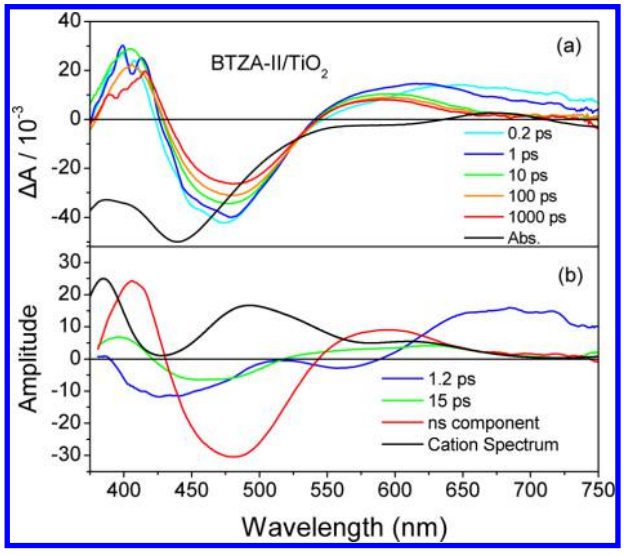

Figure 7. (a) TA spectra measured for **BTZA-II** on TiO_2 substrate at different time delays upon 400 nm excitation. The reverse absorption spectrum is also shown for comparison. (b) DADS obtained after a three exponential global analysis. The calculated radical cation spectrum is shown in (b).

The early TA spectra in $CHCl_3$ + DBU are dominated by a broad negative band below 570 nm, due to the bleach of the ground-state population (GSB) and to SE and by a positive band above 570 nm that can be ascribed to excited-state absorption (ESA). The SE band apparently decreases and shifts to longer wavelength with time, whereas the ESA band decreases as well but shifts to shorter wavelengths. The TA dynamics could be well reproduced with the sum of three exponential functions (Table 3). The two shortest time constants, 2.8 and 9.3 ps, are associated with the red shift of the SE band and can be ascribed to solvent/vibrational relaxation. The third time constant, >1000 ps, associated with the recovery of the ground-state population, is assigned to the decay of the relaxed excited state. The blue shift of the ESA band could be explained, at least partially, by the changing overlap of the SE and ESA bands with time. Additionally, the blue shift of the ESA band could also be explained by an S_1 state being more polar than the S_n state and thus an increase of the S_n–S_1 energy gap upon solvation.

In order to compare the photodynamics of the anionic form with that of the neutral one, the TA spectra of **BTZA-II** have also been measured in $CHCl_3$ solution without DBU, and the results are shown in Figures S3a and S3b (Supporting Information). The spectra are qualitatively similar to those shown in Figure 5a and can be interpreted likewise, i.e., by relaxation of an excited state with substantial CT character, indicating that addition of DBU has only a rather modest effect on the shape and temporal evolution of TA spectra. The differences in shape are due, at least partially, to the small band shift observed in the steady-state absorption and emission spectra upon addition of DBU. The DADS and time constants are also very close (Figure 5b and Figure S3b, Supporting Information), pointing to very similar excited-state dynamics.

The TA spectra of the other two sensitizers, **BTZA-I** and **BTZA-III**, in $CHCl_3$ with DBU are presented in Figures S4 and S5 (Supporting Information) and show features similar to those of **BTZA-II**. In the case of **BTZA-III**, a triple-exponential function was, however, not enough to properly reproduce the temporal evolution, and the sum of four exponential functions had to be used. The first two (1.4 and 5.3 ps) and the last time constants (>1000 ps) as well as their DADS are very similar to those obtained for **BTZA-II**.

The TA spectra of **BTZA-II** on Al_2O_3 (Figure 6a) show a GSB band around 460 nm which is at longer wavelengths compared to the steady-state absorption spectrum. In addition, a small contribution of SE is observed at short time delays between 515 and 550 nm, which is rapidly quenched either because of energy transfer to energetically lower-lying aggregates or because of electron injection into trap states (*vide infra*). Regarding the positive part of the spectra, a broad photoinduced absorption band (from 550 to 750 nm) is present in the early spectra. This band, which is assigned to an unrelaxed excited state, relaxes to generate a new positive band ranging from 510 to 650 nm, with a maximum at ~550 nm. Besides, a positive band also appears below 400 nm, i.e., close to the main absorption band of the dye radical cation. Its presence suggests that electron injection from the dye to Al_2O_3 is operative. Since the cation band at 400 nm is close to the excitation wavelength, additional TA spectra were recorded

Table 3. Parameters of TA Dynamics for the Three Sensitizers in Different Environments upon Excitation at 400 nm[a,b]

		$CHCl_3$ + DBU				Al_2O_3			TiO_2		
λ_{exc} (nm)	dye	τ_1 (ps)	τ_2 (ps)	τ_3 (ps)	τ_4 (ps)	τ_1 (ps)	τ_2 (ps)	τ_3 (ps)	τ_1 (ps)	τ_2 (ps)	τ_3
400	**BTZA-I**	2.4	8.2		>1000	1.6	29	>1000	1.3	31	ns component
	BTZA-II	2.8	9.3		>1000	1.5	28	>1000	1.2	15	ns component
	BTZA-III	1.4	5.3	48	>1000	2.2	100	>1000	1.5	22	ns component

[a]The parameters were obtained after multiexponential global analysis. [b]The error on the TA time constants is estimated to be 10%.

dx.doi.org/10.1021/jp509971q | J. Phys. Chem. C 2014, 118, 28509–28519

upon 505 nm excitation (Figure S6a, Supporting Information). They are almost identical to those measured upon excitation at 400 nm, confirming the existence of the cation band at $\lambda < 400$ nm. Thus, knowing that the dye cation is generated in Al_2O_3 and considering the calculated radical cation spectra, we attribute the ~550 nm TA band to overlapping signals coming from the relaxed excited state and the dye cation. The time evolution of the TA spectra could be reproduced using the sum of a three exponential function with 1.5, 28 and >1000 ps time constants, and the DADS are shown in Figure 6b. The first two components are associated with the decay of the unrelaxed excited state. However, the transient absorption signal at 390 nm also exhibits fast decay components. Therefore, the latter could also be associated with the decay of the cation band due to fast recombination of the injected electrons with the cations. Finally, the longest >1000 ps component is associated with a slow decay of the cation band.

The TA spectra measured for **BTZA-II** on TiO_2 (Figure 7a) upon 400 nm excitation have also been analyzed globally, and the time constants were found to be 1.2 and 15 ps together with a long ns component. The DADS are presented in Figure 7b. Five important features are obvious in these TA spectra: (i) SE is totally absent; (ii) the radical cation band is again observed at ~410 nm and decays on a longer time scale than in Al_2O_3 (ns component); (iii) the unrelaxed excited state decays faster than in Al_2O_3; (iv) the band at 600 nm is now very long-lived compared to Al_2O_3; and (v) the GSB recovery is very slow. The bleach band again exhibits a large shift compared to the steady-state absorption spectrum of the dye on TiO_2, which could be possibly due to the Stark effect produced by the local electric field generated after the electron injection.[6,17] In addition, the calculated cationic band at ~390 nm (Figure 2e) is shifted to ~410 nm in the experimental TA spectra (Figure 7a). The above-mentioned features are also present in the corresponding TA spectra of **BTZA-II** on TiO_2 upon 505 nm excitation, which are shown in Figure S6b (Supporting Information).

The TA spectra measured for **BTZA-I** and **BTZA-III** on Al_2O_3 and TiO_2 upon excitation at 400 nm are presented in Figures S7 and S8 (Supporting Information). In general, these spectra show features similar to those measured for **BTZA-II**. However, the radical cation band in Al_2O_3 is not clearly detected in the case of **BTZA-I** and **BTZA-III** because of increased scattering of the excitation light (thereby, the region below 410 nm is not shown in the TA spectra of Al_2O_3; cf. Figures S7a and S8a, Supporting Information). In order to observe the cationic band more clearly, TA measurements with excitation at 505 nm have also been performed for **BTZA-III** on Al_2O_3 and TiO_2 and are presented in Figures S9a and S9b (Supporting Information), respectively. They unambiguously show the generation of the cation band at ~410 nm in both Al_2O_3 and TiO_2. TA measurements with excitation at 505 nm could not be performed for **BTZA-I** since it does not absorb at this wavelength.

Selected TA time profiles at wavelengths corresponding to the unrelaxed band (720 nm) and the cationic band (~400 nm) are compared for **BTZA-II** on Al_2O_3 and TiO_2 in Figures 8a and 8b. On TiO_2, the unrelaxed band decays, and the cation band rises on a similar time scale suggesting that these phenomena are closely linked. The cations are generated on a <200 fs time scale as well as on a ~1 ps time scale. This agrees with the TRF dynamics, which exhibits ultrafast as well as picosecond dynamics. On Al_2O_3, the cations are entirely

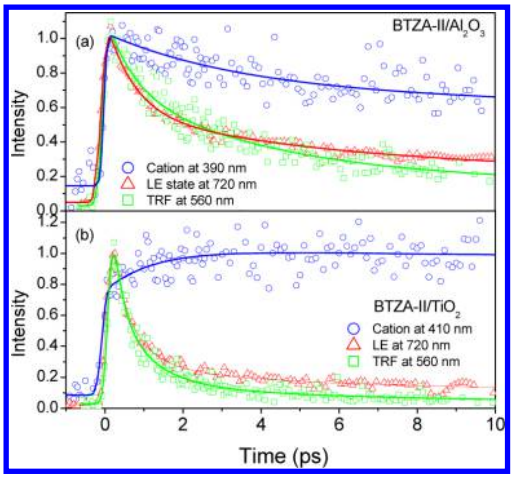

Figure 8. TA dynamics of the unrelaxed band (720 nm) and radical cation band (410 and 390 nm) of **BTZA-II** on (a) Al_2O_3 and (b) TiO_2. The TRF dynamics is also shown for comparison.

generated within the IRF. The ultrafast generation of cations in Al_2O_3 is in agreement with the observation of ultrafast decay components in the TRF experiments, especially at short detection wavelengths. The absence of additional rising components on the picosecond time scale is due to the immediate recombination of the initially injected electrons with the dye cations, making the instantaneous population of slowly generated cations too small to be detectable. Another important feature shown in Figures 8a and 8b is the comparison of the TRF dynamics (detected at the maxima of the fluorescence spectra) with those of the unrelaxed band obtained by TA spectroscopy. It is obvious that in both Al_2O_3 and TiO_2 samples the dynamics within the first 10 ps are very similar.

It is important to note that the cation band located at around 400 nm decays much faster in Al_2O_3 than in TiO_2. The long-range dynamics of this band in TiO_2 and Al_2O_3, shown in Figures 9a and 9b for **BTZA-II** and **BTZA-III**, points to multiexponential recombination.[58,59] The faster decay in Al_2O_3 is due to the fact that trapped electrons cannot diffuse through the mesoporous Al_2O_3 material and, therefore, readily

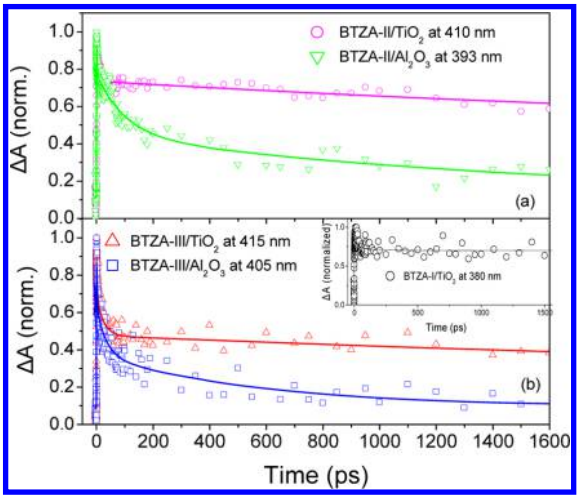

Figure 9. TA dynamics of the cation band of (a) **BZTA-II** and (b) **BZTA-III** on TiO_2 and Al_2O_3, upon 505 nm excitation. The inset shows the dynamics of the cation band of **BTZA-I** on TiO_2 upon 400 nm excitation.

dx.doi.org/10.1021/jp509971q | J. Phys. Chem. C 2014, 118, 28509−28519

recombine with the dye cations to repopulate the neutral ground state. However, in the case of TiO_2, the injected electrons have an increased possibility to become free electrons and then diffuse into the conduction band. Another conclusion derived from Figures 9a and 9b is that, in TiO_2 samples, **BTZA-II** cations live longer than those derived from **BTZA-III**, indicating a slower recombination with **BTZA-II**, which is beneficial as far as solar cell efficiency is concerned. The dynamics of the cation band of **BTZA-I** on TiO_2 is presented in the inset of Figure 9b, indicating that this sensitizer also exhibits slower recombination than **BTZA-III** but similar to **BTZA-II**. Although our experimental results do not probe the slow dynamics of recombination and accurate determination of the cation lifetime cannot be made, the above conclusions are derived by comparing the signal of the cation band of **BTZA-I**, **BTZA-II** and **BTZA-III** at long times.

An important difference between the TA spectra measured for dye-sensitized TiO_2 and Al_2O_3 thin films is the fact that the GSB band experiences a gradual red-shift in TiO_2, while this is not observed in Al_2O_3 (Figures 10a and 10b). This indicates a

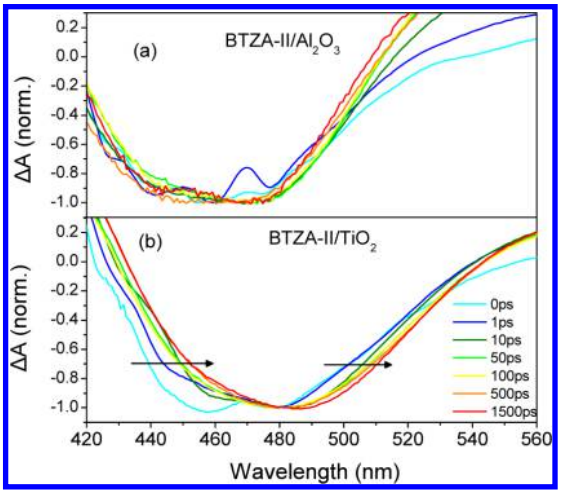

Figure 10. Time evolution of the ground-state bleach measured for **BTZA-II** on (a) Al_2O_3 and (b) TiO_2.

gradual establishment of a Stark effect as electrons are injected to the TiO_2 nanocrystalline material. The lack of this transient shift in Al_2O_3 is associated with more efficient recombination of the electrons with the cations in Al_2O_3 than in TiO_2. The understanding of the influence of Stark effects in DSSCs is of major importance and has been intensely studied in recent years both experimentally and theoretically.[6,11,17,60−62] Specifically, Bairu et al.[6] have reported a similar red-shift of the bleach band for another D-π-A sensitizer on TiO_2 and attributed this to the influence of the injected electrons and cations at early times that shift the bleach band to shorter wavelengths. However, measurements on a reference substrate, such as Al_2O_3, were missing in that work. Similar results have also been reported by Oum et al., who have also used TA spectroscopy to investigate the photodynamics in dye-coated TiO_2 and ZrO_2 samples, the latter being used as a reference material. They have detected similar early time behavior in both materials, indicating that electron injection to ZrO_2 is also operative.[11,17] However, at longer times no transient Stark effects have been observed in ZrO_2, in agreement with our own results.

Transient Absorption Dynamics in the IR. Figures 11a and 11b show the short- and long-range dynamics of the TA in

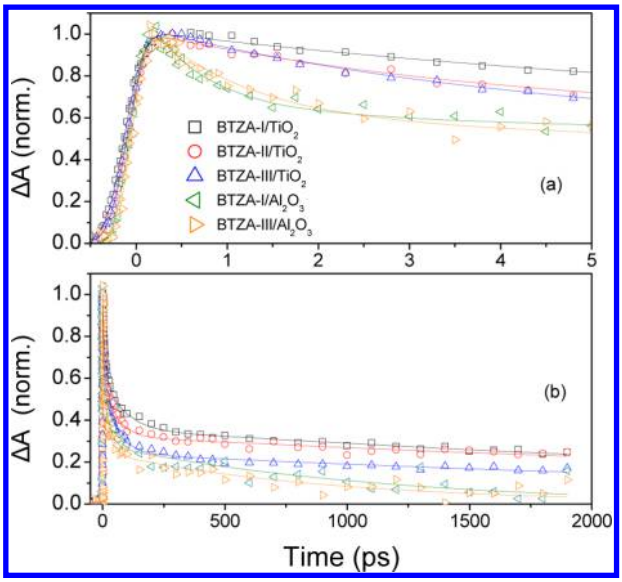

Figure 11. Normalized IR TA dynamics of the injected electron at 4000 nm upon 400 nm excitation of the dye time-resolved IR dynamics on a short (a) and long (b) time scale. Excitation is at 400 nm and detection at 4000 nm.

the IR, i.e., 4000 nm, where injected electrons in the conduction band are expected to absorb.[63−65] Excitation was performed at 400 nm. The rise of the electron absorption band is similar for the three compounds and is within the IRF (~300 fs) indicating ultrafast electron injection for all three dyes in agreement with the TRF results on TiO_2. Additionally, the absence of a slow rising injected-electron dynamics reveals that intermediate electron−cation complexes are not formed. It is interesting to note that a small but measurable TA signal was observed even for Al_2O_3 samples but only with **BTZA-I** and **BTZA-III**. In all cases, the signal from the Al_2O_3 samples was 10−20 times smaller than that measured for TiO_2. The longer time scale dynamics of the IR TA has been analyzed with a three exponential function, and the results are presented in Table S2 (Supporting Information). They present two important features: (a) The intensity in Al_2O_3 decays much faster than in TiO_2, indicating faster recombination of the injected electrons with the dye cations. This result is in agreement with the faster decay of the cations in Al_2O_3 than in TiO_2 found by visible TA. (b) The remaining population of electrons after 1.9 ns is smaller for **BTZA-III** than for the other dyes. This points to a faster charge recombination in the case of **BTZA-III**, which is also in agreement with the conclusions derived from visible TA measurements.

It should be noted here that the decay of the IR signal is not only due to the recombination of the injected electrons with the dye cations but arises also from the relaxation of electrons down the conduction band or trap states.[66,67] In order to clarify which mechanism is responsible for the decay, we compare in Figures 12a and 12b the longer time scale dynamics of the cations and injected electrons measured for **BTZA-III** on Al_2O_3 and TiO_2. On Al_2O_3, the IR and the cation signals decay very similarly, indicating that recombination is the most important decay mechanism. On TiO_2, on the other hand, the decay of the IR signal is much faster than that of the cations, revealing that the population of injected electrons experiences not only recombination but also relaxation. The relaxation of the injected electrons down the conduction band is the reason

dx.doi.org/10.1021/jp509971q | J. Phys. Chem. C 2014, 118, 28509−28519

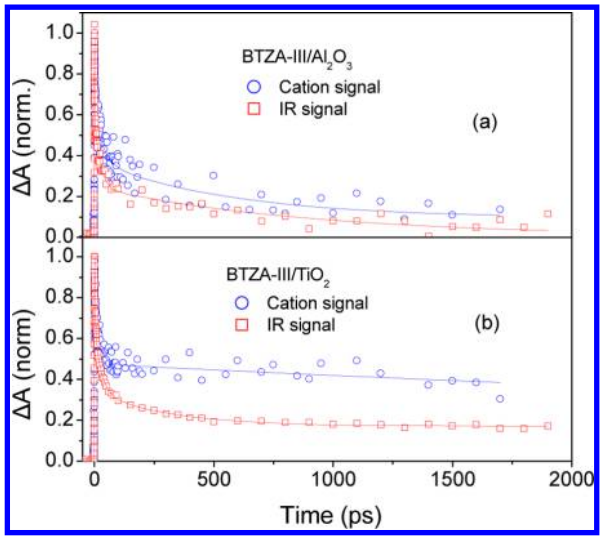

Figure 12. Comparison of the dynamics of the cation and IR TA signals measured for **BTZA-III** on (a) Al_2O_3 and (b) TiO_2 films.

why we do not observe a rise of the IR signal in TiO_2 samples within the first 2 ps, as in the case of the radical cation (Figure 8b).

Overall, the comparison of the photodynamics of the three sensitizers using various time-resolved techniques, as described above, leads to the conclusion that the differences in the structures of the sensitizers do not play a very significant role in electron injection, which always takes place on a <200 fs time scale. The main difference among the three sensitizers is the recombination rate, which is highest for **BTZA-III**, while in the other two sensitizers it is slower and almost similar to each other. The faster recombination with **BTZA-III** may be due to the presence of the methoxy groups on the triphenyl moiety that increase the electron-donating properties of this dye compared to the other two. This should lead to a reduction of the driving force for charge recombination and, thus, to a faster recombination as predicted by Marcus electron transfer theory for the inverted regime.[68] So, although **BTZA-III**'s absorption spectrum covers a significant part of the visible spectrum, the increased recombination rate is expected to have a detrimental role in solar cell efficiency. Solar cell characterization of the three compounds is underway in our laboratories and will be the subject of another publication.

CONCLUSIONS

The photophysics and electron injection dynamics of three novel D-π-A organic sensitizers have been examined using a combination of steady-state, femtosecond time-resolved fluorescence spectroscopy and femtosecond transient absorption spectroscopy in the visible and IR regions. The dipolar sensitizers contain a triphenylamine moiety (with or without additional methoxy substituents) connected via an ethenylene or an ethynylene π-spacer to benzothiazole with a cyano-acrylic acid functionality as the acceptor. The time-resolved studies have been performed in $CHCl_3$ and $CHCl_3$ + DBU solutions and on TiO_2 and Al_2O_3 films. Time-resolved fluorescence and transient absorption measurements on TiO_2 have shown an ultrafast electron injection for all three dyes, indicating that the differences in the chemical structures do not influence the injection process. The transient absorption spectra upon excitation at 400 and 505 nm provide sufficient evidence for the generation of dye radical cations in the dye-coated TiO_2 films as well as in the Al_2O_3 ones. The radical cations are long-lived in TiO_2 because of slow back electron transfer. Additionally, a transient red shift of the bleaching band is observed and is attributed to a transient Stark effect. The cation lifetime in Al_2O_3 is much reduced compared to that in TiO_2, indicating a fast recombination of the trapped electrons with the dye cations. Finally, femtosecond transient absorption experiments in the IR region, probing the population of the injected electrons, point to an ultrafast generation of electrons in TiO_2 as well as in Al_2O_3 (but to a much smaller extent) and to a faster recombination in Al_2O_3 in agreement with the transient absorption measurements in the visible. The recombination rate of injected electrons was found to be similar for **BTZA-I** and **BTZA-II** indicating that it does not depend on whether there is a triple or double bond spacer. However, a faster recombination of the injected electrons was observed for the dye with additional methoxy substituents coupled to the triphenylamine moiety (**BTZA-III**), which is expected to play a detrimental role in its solar cell efficiency.

ASSOCIATED CONTENT

Supporting Information

Supplemental data including details on the synthesis of the compounds, time-resolved dynamics, and transient absorption spectra of **BTZA-I**, **BTZA-II**, and **BTZA-III** in different environments. This material is available free of charge via the Internet at http://pubs.acs.org.

AUTHOR INFORMATION

Corresponding Authors

*E-mail: fakis@upatras.gr.
*E-mail: peter.hrobarik@tu-berlin.de.
*E-mail: eric.vauthey@unige.ch.

Notes

The authors declare no competing financial interest.

ACKNOWLEDGMENTS

M.F. gratefully acknowledges financial support from the Swiss National Science Foundation via the International short visits funding instrument (no. IZK0Z2_149047), and P.H. thanks the Alexander von Humboldt Foundation for a research fellowship. The synthetic work has been supported by the Slovak Research and Development Agency under contracts APVV-0424-10 and APVV-0622-12 and by the R&D Operational Programme "NanoNet" funded by the European Regional Development Fund. The research of E.S. has been cofinanced by the European Union (European Social Fund – ESF) and Greek national funds through the Operational Program "Education and Lifelong Learning" of the National Strategic Reference Framework (NSRF) - Research Funding Program: THALES, MIS: 377756. Support from the Swiss National Science Foundation via project no. 200020-147098 and the University of Geneva is also acknowledged.

REFERENCES

(1) Yella, A.; Lee, H.-W.; Tsao, H. N.; Yi, C.; Chandiran, A. K.; Nazeeruddin, M. K.; Diau, E. W.-G.; Yeh, C.-Y.; Zakeeruddin, S. M.; Grätzel, M. Porphyrin-Sensitized Solar Cells with Cobalt (II/III) Based Redox Electrolyte Exceed 12% Efficiency. *Science* **2011**, *334*, 629–634.

(2) Hardin, B. E.; Snaith, H. J.; McGehee, M. D. The Renaissance of Dye-Sensitized Solar Cells. *Nat. Photonics* **2012**, *6*, 162–169.

(3) Listorti, A.; O'Regan, B.; Durrant, J. R. Electron Transfer Dynamics in Dye-Sensitized Solar Cells. *Chem. Mater.* **2011**, *23*, 3381−3399.
(4) Asbury, J. B.; Hao, E.; Wang, Y.; Ghosh, H. N.; Lian, T. Ultrafast Electron Transfer Dynamics from Molecular Adsorbates to Semiconductor Nanocrystalline Thin Films. *J. Phys. Chem. B* **2001**, *105*, 4545−4557.
(5) Wang, L.; Wang, H.-Y.; Fang, H.-H.; Wang, H.; Yang, Z.-Y.; Gao, B.-R.; Chen, Q.-D.; Han, W.; Sun, H.-B. Universal Electron Injection Dynamics at Nanointerfaces in Dye-Sensitized Solar Cells. *Adv. Funct. Mater.* **2012**, *22*, 2783−2791.
(6) Bairu, S. G.; Mghanga, E.; Hasan, J.; Kola, S.; Rao, V. J.; Bhanuprakash, K.; Giribabu, L.; Wiederrecht, G. P.; Da Silva, R.; Rego, L. G. C.; et al. Ultrafast Interfacial Charge-Transfer Dynamics in a Donor-π-Acceptor Chromophore Sensitized TiO_2 Nanocomposite. *J. Phys. Chem. C* **2013**, *117*, 4824−4835.
(7) Rohwer, E.; Richter, C.; Heming, N.; Strauch, K.; Litwinski, C.; Nyokong, T.; Schlettwein, D.; Schwoerer, H. Ultrafast Photodynamics of the Indoline Dye D149 Adsorbed to Porous ZnO in Dye-Sensitized Solar Cells. *ChemPhysChem* **2013**, *14*, 132−139.
(8) Zhang, J.; Yao, Z.; Cai, Y.; Yang, L.; Xu, M.; Li, R.; Zhang, M.; Donga, X.; Wang, P. Conjugated Linker Correlated Energetics and Kinetics in Dithienopyrrole Dye-Sensitized Solar Cells. *Energy Environ. Sci.* **2013**, *6*, 1604−1614.
(9) Qin, P.; Wiberg, J.; Gibson, P.; Linder, P.; Li, P.; Brinck, P.; Hagfeldt, P.; Albinsson, P.; Sun, L. C. Synthesis and Mechanistic Studies of Organic Chromophores with Different Energy Levels for p-type Dye-Sensitized Solar Cells. *J. Phys. Chem. C* **2010**, *114*, 4738−4748.
(10) Fakis, M.; Stathatos, E.; Tsigaridas, B.; Giannetas, V.; Persephonis, P. Femtosecond Decay and Electron Transfer Dynamics of the Organic Sensitizer D149 and Photovoltaic Performance in Quasi-Solid-State Dye-Sensitized Solar Cells. *J. Phys. Chem. C* **2011**, *115*, 13429−13437.
(11) Oum, K.; Lohse, P. W.; Flender, O.; Klein, J. R.; Scholz, M.; Lenzer, T.; Du, J.; Oekermann, T. Ultrafast Dynamics of the Indoline Dye D149 on Electrodeposited ZnO and Sintered ZrO_2 and TiO_2 Thin Films. *Phys. Chem. Chem. Phys.* **2012**, *14*, 15429−15437.
(12) Juozapavicius, M.; Kaucikas, M.; Van Thor, J. J.; O'Regan, B. C. Observation of Multiexponential Pico- to Subnanosecond Electron Injection in Optimized Dye-Sensitized Solar Cells with Visible-Pump Mid-Infrared-Probe Transient Absorption Spectroscopy. *J. Phys. Chem. C* **2013**, *117*, 116−123.
(13) Ziolek, M.; Martín, C.; Sun, L.; Douhal, A. Effect of Electrolyte Composition on Electron Injection and Dye Regeneration Dynamics in Complete Organic Dye Sensitized Solar Cells Probed by Time-Resolved Laser Spectroscopy. *J. Phys. Chem. C* **2012**, *116*, 26227−26238.
(14) Sunahara, K.; Furube, A.; Katoh, R.; Mori, S.; Griffith, M. J.; Wallace, G. G.; Wagner, P.; Officer, D. L.; Mozer, A. J. Coexistence of Femtosecond- and Nonelectron-Injecting Dyes in Dye-Sensitized Solar Cells: Inhomogeniety Limits the Efficiency. *J. Phys. Chem. C* **2011**, *115*, 22084−22088.
(15) Pijpers, J. J. H.; Ulbricht, R.; Derossi, S.; Reek, J. N. H.; Bonn, M. Picosecond Electron Injection Dynamics in Dye-Sensitized Oxides in the Presence of Electrolyte. *J. Phys. Chem. C* **2011**, *115*, 2578−2584.
(16) Koops, S. E.; O' Regan, B. C.; Barnes, P. R. F.; Durrant, J. R. Parameters Influencing the Efficiency of Electron Injection in Dye-Sensitized Solar Cells. *J. Am. Chem. Soc.* **2009**, *131*, 4808−4818.
(17) Oum, K.; Lohse, P. W.; Klein, J. R.; Flender, O.; Scholz, M.; Hagfeldt, A.; Boschloo, G.; Lenzer, T. Photoinduced Ultrafast Dynamics of the Triphenylamine-based Organic Sensitizer D35 on TiO_2, ZrO_2 and in Acetonitrile. *Phys. Chem. Chem. Phys.* **2013**, *15*, 3906−3916.
(18) Ziolek, M.; Cohen, B.; Yang, X.; Sun, L.; Paulose, M.; Varghese, O. K.; Grimes, C. A.; Douhal, A. Femtosecond to Millisecond Studies of Electron Transfer Processes in a Donor-(π-spacer)-acceptor Series of Organic Dyes for Solar Cells Interacting with Titania Nanoparticles and Ordered Nanotube Array Films. *Phys. Chem. Chem. Phys.* **2012**, *14*, 2816−2831.
(19) Teuscher, J.; Decoppet, J.-D.; Punzi, A.; Zakeeruddin, S. M.; Moser, J.-E.; Gratzel, M. Photoinduced Interfacial Electron Injection Dynamics in Dye Sensitized Solar Cells under Photovoltaic Operating Conditions. *J. Phys. Chem. Lett.* **2012**, *3*, 3786−3790.
(20) Wiberg, J.; Marinado, T.; Hagberg, D. P.; Sun, L.; Hagfeldt, A.; Albinsson, B. Distance and Driving Force Dependencies of Electron Injection and Recombination Dynamics in Organic Dye Sensitized Solar Cells. *J. Phys. Chem. B* **2010**, *114*, 14358−14363.
(21) Stockwell, D.; Yang, Y.; Huang, J.; Anfuso, C.; Huang, Z.; Lian, T. Comparison of Electron Transfer Dynamics from Coumarin 343 to TiO_2, SnO_2 and ZnO Nanocrystalline Thin Films: Role of Interface-Bound Charge-Separated Pairs. *J. Phys. Chem. C* **2010**, *114*, 6560−6566.
(22) Myllyperkio, P.; Manzoni, C.; Polli, D.; Cerullo, G.; Korppi-Tommola, J. Electron Transfer from Organic Aminophenyl Acid Sensitizers to Titanium Dioxide Nanoparticle Films. *J. Phys. Chem. C* **2009**, *113*, 13989−13992.
(23) Bram, O.; Cannizzo, A.; Chergui, M. Ultrafast Fluorescence Studies of Dye Sensitized Solar Cells. *Phys. Chem. Chem. Phys.* **2012**, *14*, 7934−7937.
(24) Lu, H.-P.; Tsai, C.-Y.; Yen, W.-N.; Hsieh, C.-P.; Lee, C.-W.; Yeh, C.-Y.; Diau, E.W.-G. Control of Dye Aggregation and Electron Injection for Highly Efficient Porphyrin Sensitizers Adsorbed on Semiconductor Films with Varying Ratios of Coadsorbate. *J. Phys. Chem. C* **2009**, *113*, 20990−20997.
(25) Lin, C.-H.; Lo, C.-F.; Luo, L.; Lu, H.-P.; Hung, C.-S.; Diau, E.W.-G. Design and Characterization of Novel Porphyrins with Oligo(Phenylethynyl) Links of Varied Length for Dye-Sensitized Solar Cells: Synthesis and Optical, Electrochemical, and Photovoltaic Investigation. *J. Phys. Chem. C* **2009**, *113*, 755−764.
(26) Fakis, M.; Dori, M.; Stathatos, E.; Chou, H.-H.; Yen, Y.-S.; Lin, J.-L.; Giannetas, V.; Persephonis, P. Electron Injection in TiO_2 Films and Quasi-Solid State Solar Cells Sensitized with a Dipolar Fluorene Organic Dye. *J. Photochem. Photobiol. A: Chem.* **2013**, *251*, 18−24.
(27) Ziolek, M.; Tacchini, I.; Martinez, M. T.; Yang, X.; Sun, L.; Douhal, A. A Photo-Induced Electron Transfer Study of an Organic Dye Anchored on the Surfaces of TiO_2 Nanotubes and Nanoparticles. *Phys. Chem. Chem. Phys.* **2011**, *13*, 4032−4044.
(28) Cappel, U. B.; Feldt, S. M.; Schoneboom, J.; Hagfeldt, A.; Boschloo, G. The Influence of Local Electric Fields on Photoinduced Absorption in Dye-Sensitized Solar Cells. *J. Am. Chem. Soc.* **2010**, *132*, 9096−9101.
(29) Mishra, A.; Fischer, M. K. R.; Bäuerle, P. Metal-Free Organic Dyes for Dye-Sensitized Solar Cells: From Structure: Property Relationships to Design Rules. *Angew. Chem., Int. Ed.* **2009**, *48*, 2474−2499.
(30) Chen, C.-H.; Hsu, Y.-Y.; Chou, H.-H.; Justin Thomas, K. R.; Lin, J. T.; Hsu, C.-P. Dipolar Compounds Containing Fluorene and a Heteroaromatic Ring as the Conjugating Bridge for High-Performance Dye-Sensitized Solar Cells. *Chem.—Eur. J.* **2010**, *16*, 3184−3193.
(31) Hagberg, D. P.; Yum, J. H.; Lee, H.; De Angelis, D.; Marinado, T.; Karlsson, K. M.; Humphry-Baker, R.; Sun, L.; Hagfeldt, A.; Gratzel, M.; et al. Molecular Engineering of Organic Sensitizers for Dye-sensitized Solar Cell Applications. *J. Am. Chem. Soc.* **2008**, *130*, 6259−6266.
(32) Preat, J.; Michaux, C.; Jacquemin, D.; Perpete, E. A. Enhanced Efficiency of Organic Dye-sensitized Solar Cells: Triphenylamine Derivatives. *J. Phys. Chem. C* **2009**, *113*, 16821−16833.
(33) Ren, X.; Jiang, S.; Cha, M.; Zhou, G.; Wang, Z. S. Thiophene-Bridged Double D-π-A Dye for Efficient Dye-Sensitized Solar Cell. *Chem. Mater.* **2012**, *24*, 3493−3499.
(34) Wan, Z.; Jia, C.; Duan, Y.; Zhou, L.; Lin, Y.; Shi, Y. Phenothiazine−triphenylamine Based Organic Dyes Containing Various Conjugated Linkers for Efficient Dye-sensitized Solar Cells. *J. Mater. Chem.* **2012**, *22*, 25140−25147.
(35) Kozma, E.; Concina, I.; Braga, A.; Borgese, L.; Depero, L. E.; Vomiero, A.; Sberveglieri, G.; Catellani, M. Metal-free Organic

Sensitizers with a Sterically Hindered Thiophene Unit for Efficient Dye-sensitized Solar Cells. *J. Mater. Chem.* **2011**, *21*, 13785−13788.
(36) Hara, K.; Sato, T.; Katoh, R.; Furube, A.; Yoshihara, T.; Murai, M.; Kurashige, M.; Ito, S.; Shinpo, A.; Suga, S.; et al. Novel Conjugated Organic Dyes for Efficient Dye-Sensitized Solar Cells. *Adv. Funct. Mater.* **2005**, *15*, 246−252.
(37) Howie, W. H.; Claeyssens, F.; Miura, H.; Peter, L. M. Characterization of Solid-State Dye-Sensitized Solar Cells Utilizing High Absorption Coefficient Metal-Free Organic Dyes. *J. Am. Chem. Soc.* **2008**, *130*, 1367−1375.
(38) Baheti, A.; Singh, P.; Lee, C.-P.; Justin Thomas, K. R.; Ho, K.-C. 2,7-Diaminofluorene-Based Organic Dyes for Dye-Sensitized Solar Cells: Effect of Auxiliary Donor on Optical and Electrochemical Properties. *J. Org. Chem.* **2011**, *76*, 4910−4920.
(39) Cao, D.; Peng, J.; Hong, Y.; Fang, X.; Wang, L.; Meier, H. Enhanced Performance of the Dye-Sensitized Solar Cells with Phenothiazine-Based Dyes Containing Double D−A Branches. *Org. Lett.* **2011**, *13*, 1610−1613.
(40) Hong, Y.; Liao, J.-Y.; Cao, D.; Zang, X.; Kuang, D.-B.; Wang, L.; Meier, H.; Su, C.-Y. Organic Dye Bearing Asymmetric Double Donor-π-Acceptor Chains for Dye-Sensitized Solar Cells. *J. Org. Chem.* **2011**, *76*, 8015−8021.
(41) Zeng, J.; Zhang, T. L.; Zang, X. F.; Kuang, D. B.; Meier, H.; Cao, D. R. D-A-π-A Organic Sensitizers Containing a Benzothiazole Moiety as an Additional Acceptor for Use in Solar Cells. *Sci. China Chem.* **2013**, *56*, 505−513.
(42) Hrobárik, P.; Zahradník, P.; Fabian, W. M. F. Computational Design of Benzothiazole-Derived Push-Pull Dyes with High Molecular Quadratic Hyperpolarizabilities. *Phys. Chem. Chem. Phys.* **2004**, *6*, 495−502.
(43) Hrobárik, P.; Sigmundová, I.; Zahradník, P. Preparation of Novel Push-Pull Benzothiazoles with Reverse Polarity: Compounds with Potential Nonlinear Optical Application. *Synthesis-Stuttgart* **2005**, 600−604.
(44) Hrobárik, P.; Sigmundová, I.; Zahradník, P.; Kasák, P.; Arion, V.; Franz, E.; Clays, K. Molecular Engineering of Benzothiazolium Salts with Large Quadratic Hyperpolarizabilities: Can Auxiliary Electron-Withdrawing Groups Enhance Nonlinear Optical Responses? *J. Phys. Chem. C* **2010**, *114*, 22289−22302.
(45) Hrobáriková, V.; Hrobárik, P.; Gajdoš, P.; Fitilis, I.; Fakis, M.; Persephonis, P.; Zahradník, P. Benzothiazole-Based Fluorophores of Donor-π-Acceptor-π-Donor Type Displaying High Two-Photon Absorption. *J. Org. Chem.* **2010**, *75*, 3053−3068.
(46) Hrobárik, P.; Hrobáriková, V.; Sigmundová, I.; Zahradník, P.; Fakis, M.; Polyzos, I.; Persephonis, P. Benzothiazoles with Tunable Electron-Withdrawing Strength and Reverse Polarity: A Route to Triphenylamine-Based Chromophores with Enhanced Two-Photon Absorption. *J. Org. Chem.* **2011**, *76*, 8726−8736.
(47) Costa, S. P. G.; Batista, R. M. F.; Cardoso, P.; Belsley, M.; Raposo, M. M. M. 2-Arylthienyl-Substituted 1,3-Benzothiazoles as New Nonlinear Optical Chromophores. *Eur. J. Org. Chem.* **2006**, 3938−3946.
(48) Hrobárik, P.; Hrobáriková, V.; Semak, V.; Kasák, P.; Rakovský, E.; Polyzos, I.; Fakis, M.; Persephonis, P. Quadrupolar Benzobisthiazole-Cored Arylamines as Highly Efficient Two-Photon Absorbing Fluorophores. *Org. Lett.* **2014**, DOI: 10.1021/ol503137p.
(49) Frisch, M. J.; Trucks, G. W.; Schlegel, H. B.; Scuseria, G. E.; Robb, M. A.; Cheeseman, J. R.; Scalmani, G.; Barone, V.; Mennucci, B.; Petersson, G. A.; et al. *Gaussian 09*, revision A.02; Gaussian, Inc.: Wallingford, CT, 2009.
(50) Yanai, T.; Tew, D. P.; Handy, N. C. A New Hybrid Exchange-Correlation Functional Using the Coulomb Attenuating Method (CAM-B3LYP). *Chem. Phys. Lett.* **2004**, *393*, 51−57.
(51) Tomasi, J.; Mennucci, B.; Cammi, R. Quantum Mechanical Continuum Solvation Models. *Chem. Rev.* **2005**, *105*, 2999−3093.
(52) Duvanel, G.; Banerji, N.; Vauthey, E. Excited-State Dynamics of Donor−Acceptor Bridged Systems Containing a Boron−Dipyrromethene Chromophore: Interplay between Charge Separation and Reorientational Motion. *J. Phys. Chem. A* **2007**, *111*, 5361−5369.
(53) Banerji, N.; Duvanel, G.; Perez-Velasco, A.; Maity, S.; Sakai, N.; Matile, S.; Vauthey, E. Excited-State Dynamics of Hybrid Multichromophoric Systems: Toward an Excitation Wavelength Control of the Charge Separation Pathways. *J. Phys. Chem. A* **2009**, *113*, 8202−8212.
(54) Koch, M.; Rosspeintner, A.; Adamczyk, K.; Lang, B.; Dreyer, J.; Nibbering, E. T. J.; Vauthey, E. Real-Time Observation of the Formation of Excited Radical Ions in Bimolecular Photoinduced Charge Separation: Absence of the Marcus Inverted Region Explained. *J. Am. Chem. Soc.* **2013**, *135*, 9843−9848.
(55) Ziolek, M.; Yang, X.; Sun, L.; Douhal, A. Interrogating the Ultrafast Dynamics of an Efficient Dye for Sunlight Conversion. *Phys. Chem. Chem. Phys.* **2010**, *12*, 8098−8107.
(56) Luo, L.; Lo, C.-F.; Lin, C.-Y.; Chang, I.-J.; Diau, E. W.-G. Femtosecond Fluorescence Dynamics of Porphyrin in Solution and Solid Films: The Effects of Aggregation and Interfacial Electron Transfer between Porphyrin and TiO_2. *J. Phys. Chem. B* **2006**, *110*, 410−419.
(57) Deshpande, A. V.; Beidoun, A.; Penzkofer, A. Absorption and emission spectroscopic investigation of cyanovinyldiethylaniline dye vapors. *Chem. Phys.* **1990**, *142*, 123−131.
(58) Vinodgopal, K.; Hua, X.; Dahlgren, R. L.; Lappin, A. G.; Patterson, L. K.; Kamat, P. V. Photochemistry of $Ru(bpy)_2(dcbpy)^{2+}$ on Al_2O_3 and TiO_2 Surfaces. An Insight into the Mechanism of Photosensitization. *J. Phys. Chem.* **1995**, *99*, 10883−10889.
(59) Ramakrishna, G.; Jose, D. A.; Kumar, D. K.; Das, A.; Palit, D. K.; Ghosh, H. N. Strongly Coupled Ruthenium−Polypyridyl Complexes for Efficient Electron Injection in Dye-Sensitized Semiconductor Nanoparticles. *J. Phys. Chem. B* **2005**, *109*, 15445−15453.
(60) Ardo, S.; Sun, Y.; Staniszewski, A.; Castellanao, F. N.; Meyer, G. J. Stark Effects after Excited-state Interfacial Electron Transfer at Sensitized TiO_2 Nanocrystallites. *J. Am. Chem. Soc.* **2010**, *132*, 6696−6709.
(61) Ardo, S.; Sun, Y.; Castellano, F. N.; Meyer, G. J. Excited-State Electron Transfer from Ruthenium-Polypyridyl Compounds to Anatase TiO_2 Nanocrystallites: Evidence for a Stark Effect. *J. Phys. Chem. B* **2010**, *114*, 14596−14604.
(62) Pastore, M.; De Angelis, F. Computational Modeling of Stark Effects in Organic Dye-Sensitized TiO_2 Heterointerfaces. *J. Phys. Chem. Lett.* **2011**, *2*, 1261−1267.
(63) Yoshihara, T.; Katoh, R.; Furube, A.; Tamaki, Y.; Murai, M.; Hara, K.; Murata, S.; Arakawa, H.; Tachiya, M. Identification of Reactive Species in Photoexcited Nanocrystalline TiO_2 Films by Wide-Wavelength-Range (400−2500 nm) Transient Absorption Spectroscopy. *J. Phys. Chem. B* **2004**, *108*, 3817−3823.
(64) Szczepankiewicz, S. H.; Moss, J. A.; Hoffmann, M. R. Electron Traps and the Stark Effect on Hydroxylated Titania Photocatalysts. *J. Phys. Chem. B* **2002**, *106*, 7654−7658.
(65) Yamakata, A.; Ishibashi, T.-A.; Onishi, H. Time-resolved infrared absorption spectroscopy of photogenerated electrons in platinized TiO_2 particles. *Chem. Phys. Lett.* **2001**, *333*, 271−277.
(66) Tamaki, Y.; Hara, K.; Katoh, R.; Tachiya, M.; Furube, A. Femtosecond visible-to-IR spectroscopy of TiO_2 nanocrystalline films: Elucidation of the electron mobility before deep trapping. *J. Phys. Chem. C* **2009**, *113*, 11741−11746.
(67) Tamaki, Y.; Furube, A.; Murai, M.; Hara, K.; Katoh, R.; Tachiya, M. Dynamics of efficient electron-hole separation in TiO_2 nanoparticles revealed by femtosecond transient absorption spectroscopy under the weak-excitation condition. *Phys. Chem. Chem. Phys.* **2007**, *9*, 1453−1460.
(68) Marcus, R. A.; Sutin, N. Electron Transfer in Chemistry and Biology. *Biochim. Biophys. Acta* **1985**, *811*, 265−322.